Optimal sizing of a Hybrid Renewable Energy System: Importance of data selection with highly variable renewable energy sources

Optimal sizing of a Hybrid Renewable Energy System: importance of data selection with highly variable renewable energy sources

Jacopo Carlo Alberizzi[a,*], Joaquim Meléndez Frigola[b],
Mosè Rossi[a], Massimiliano Renzi[a]

[a]*Free University of Bozen-Bolzano, Faculty of Science and Technology, Piazza Università 1, Bozen - Bolzano – 39100, South-Tyrol, Italy*
[b]*University of Girona, Institute of Informatics and Applications, Campus Montilivi, P4 Building, Girona, E17071, Catalonia, Spain*

Abstract

The replacement of fossil fuels for producing energy with renewable sources is crucial to limit the climate change effects. However, the unpredictable nature of renewables, like sun and wind, complicates their integration within the power systems. This problem can be faced with the introduction of Hybrid Renewable Energy Systems (HRESs) where several energy sources can be incorporated. A key aspect is the assessment of the HRES configuration, which is fundamental to obtain a feasible system from both technical and economic points of view. In this paper, a novel Mixed Integer Linear Programming (MILP) optimization algorithm has been developed to design a tool capable of assessing the optimal sizing of a HRES. The algorithm has been applied to a real case study of a mountain hut located in South-Tyrol (Italy) with a hybrid system composed by solar, wind and diesel generators together with a battery storage. The algorithm compares several scenarios providing the optimal configurations of the HRES, which are characterized by different costs and energy deficits. This tool helps engineers to identify the best trade-off between costs and energy deficits in the planning phase of a HRES, still granting the demand of the users as well as the constraints.

Keywords: Hybrid Renewable Energy Systems, Mixed Integer Linear Programming, Solar Energy, Wind Energy, Diesel Engine, Battery Storage.

*Corresponding author
Email address: `jacopo.alberizzi@natec.unibz.it` (Jacopo Carlo Alberizzi)

Nomenclature

PV system

α Absorptivity of the cell [-]

β Efficiency loss coefficient of the solar cell [°C^{-1}]

η_{BOS} Balance of system efficiency [-]

η_{c} Cell efficiency [-]

$\eta_{\text{n,c}}$ Rated efficiency of the cell in STC [-]

τ transmissivity of the cell [-]

A_{eff} Net cell opening area [m^2]

E_{PV} Energy delivered by the PV system [kWh]

G Global Irradiance on the panel tilted surface [kWh/m^2]

$NOCT$ Nominal Operating Cell Temperature of the PV panel [°C]

T_{A} Ambient temperature [°C]

T_{C} Cell temperature [°C]

Wind turbine system

$\rho_{air(STC)}$ Air density in STC [kg/m^3]

ρ_{air} Air density [kg/m^3]

E_{WT} Energy delivered by the wind system [kWh]

P_R Rated power delivered by the wind turbine in STC [kW]

$P_{WT(STC)}$ Power delivered by the wind turbine in STC [kW]

P_{WT} Power delivered by the wind turbine [kW]

W_{cut-in} Cut in speed of the wind turbine [m/s]

$W_{cut-out}$ Cut out speed of the wind turbine [m/s]

W_{hub} Wind speed at hub height [m/s]

W_h Wind speed measured at the anemometer height [m/s]

W_R Wind speed corresponding to the rated power [m/s]

z_0 Surface roughness [m]

z_{hub} Hub height [m]

Diesel generator

η_{gen} Efficiency of the diesel generator [-]

ρ_{fuel} Fuel density [kg/m^3]

E_{Mot} Energy delivered by the Diesel generator [kWh]

F_C Fuel consumption [g/s]

LHV_{fuel} Lower Heating Value [MJ/kg]

P_{el} Electrical power [kW]

P_r Rated power [kW]

Battery storage

σ Self discharge rate [-]

B_C Battery capacity [kWh]

E_{batt} Energy delivered or stored [kWh]

MILP model

C_{Batt} Total NPC of a battery unit [€]

C_{PV} Total NPC of a PV unit [€]

C_{WT} Total NPC of a WT unit [€]

N_{Batt} Total number of batteries units [-]

N_{Diesel} Total number of diesel generators [-]

N_{PV} Total number of PV panels [-]

N_{WT} Total number of wind turbines [-]

NPC of the HRES

C_{fuel} Fuel cost [€]

C_{IN} Initial capital cost [€]

$C_{O\&M}$ Operation and maintenance cost [€]

C_R Replacement cost [€]

D_f Discount factor [-]

f Inflation rate [-]

i Real discount rate [-]

Other abbreviations

BOS Balance of System

E_{Load} Energy absorbed by the load [kWh]

GHG Greenhouse gas

$HRES$ Hybrid Renewable Energy System

$MILP$ Mixed Integer Linear Programming

NPC Net Present Cost

STC Standard Test Conditions

1. Introduction

The continuous development of Renewable Energy Systems (RES) has become a key aspect in many Countries all over the World with the aim of guaranteeing a clean and sustainable development, as well as to contrast the effects of the climate change. Even though the replacement of fossil fuels with renewables for producing energy is nowadays crucial, the use of traditional sources is continuously increasing. In such a context, the use of non-fossil fuels is still low for preventing this continuous growth [1]. One of the main reasons that limits the replacement of fossil fuels with renewables is their fluctuating and unpredictable nature, which complicates the integration within the power systems [2]. The characteristics of solar and wind energies may lead to an excess of energy production that would be wasted if the balance between the load requirements and the generated energy does not match. For instance, a global amount of curtailed electrical energy of 940.8 billion kWh was estimated in the year 2013 [3].

Locations that have few connections with the national grid, or those that have not been electrified so far, are typical examples where the introduction of renewables would be crucial for decreasing the environmental burden. When considering the electrification of rural areas through mini-grids, the lack of methodologies related to the assessment of the energy needs can lead to an inefficient system design. Gambino et al. [4] proposed a solution that takes into account both specific needs and context conditions, characterizing a community to be electrified. They developed a methodology that can be applied per each different case based on data collection methods, aiming to achieve a high accurate description of the electricity consumption. Hybrid Renewable Energy Systems (HRESs) are currently being developed in order to exploit the sources available in a determined area instead of adopting solutions based on convectional generators or power grid extensions, thus resulting in a more profitable use of these sources on both environmental and economic points of view [5, 6]. HRESs are outlined by different configurations: for instance, they can be composed by photovoltaic (PV) panels coupled with batteries [7], wind turbines paired with batteries [8], PV panels mated with wind turbines [9] or by coupling PV panels and wind turbines together with a Pumped Hydro Energy Storage (PHES) [10]. In addition, other configurations can be PV-wind-battery [11, 12], PV-wind-hydrogen [13], PV-wind-battery-diesel generator [14], PV-Wind-Combined Heat and Power (CHP) [15], PV-wind-biomass [16] and PV-biogas generator-PHES with battery storage [17]. Further examples can be found in [18].

When considering the installation of an off-grid HRES, one of the main challenges is the evaluation of the optimal design, which is related to the selection of the optimal number and size of the system components [19]. To achieve this goal, optimization techniques that are divided into mathematical and metaheuristic methods have to be used [20]. Mathematical methods are suitable for solving linear problems and allow engineers to obtain the exact optimal solution. On the other hand, metaheuristic methods find the optimal solution iteratively, thus requiring lower computational efforts: however, they provide an approximate solution that is not always the exact one [21]. Among the first ones, Linear Programming (LP) and Mixed Integer Linear Programming (MILP) have been widely applied to the HRESs optimization. Morais et al. [22] used this technique to compute the optimal operation scheduling of an isolated system constituted by PV panels, wind turbines and a fuel cell coupled with a storage. Ferrer et al. [23] developed a MILP model, which has been applied to a case study in Peru, in order to optimize hybrid off-grid PV-wind systems. The model computes the optimal solution considering various consumption points with the aim of minimizing the objective function that represents the initial investment cost of the system. Malheiro et al. [24] used a MILP model to design an isolated PV-wind-diesel with a battery storage where its Levelized Cost Of Energy (LCOE) has been used as objective function. Among the second ones, Genetic Algorithm (GA) and Particle Swarm Optimization (PSO) methods have been widely employed to compute the optimal sizing of HRESs. Zhao et al. [25] used a GA for a multi-objective optimization of a system composed by PV panels, wind turbines and a diesel engine coupled with a battery storage. The multi-objective optimization aimed to minimize the life-cycle cost, as well as the system pollutant emissions, and maximize the penetration of renewables. Stoppato et al. [26] developed a PSO model to optimize the cost of a PV-PHES system in a rural village located in North Nigeria.

However, HRESs have been also investigated by means of commercial software like HOMER. For instance, HOMER has been used in [27], [28] and [29] to study an off-grid PV-wind-hydro system coupled with a battery storage and a back-up diesel generator, while in [30] it was used to assess the optimal planning of a hybrid system composed by PV panels, diesel generators and a battery storage as well. Along the same line, the IHOGA [31] software was developed by the University of Zaragoza and applies optimization models, based on GA, to analyse HRESs as discussed in [32] and [33]. In several cases, the techno-economic optimization of a HRES is based on simplified assumptions that provide an optimal result but, if the external conditions vary, they can lead to either under-sized or over-sized systems. The most common assumptions regard the load profile, which is considered to be the same per each day of the year, and the shape of both solar and wind energies. Indeed, the selection of the optimal configuration of a HRES cannot be assumed as unique for an application where the daily load profile and the sources shape vary. For this reason, an assessment of possible optimal solutions can help engineers to choose the best configuration that meets the system needs.

In this work, a MILP optimization model has been developed with Matlab© [34] and applied to a case study of a mountain hut, located in the Italian region of South-Tyrol (Italy), in order to assess the optimal sizing of a PV-wind-diesel generator system together coupled with a lead-acid battery storage. The paper analyses the possibility of electrifying the hut through a HRES: in this case, the high level of complexity related to the system optimization regards the strong variability of the load, as well as the high level of fluctuations of both sun and wind sources. The main novelty of the work is the methodology adopted to assess how the configuration of a HRES, thus the optimal sizing, can vary depending on the variability of both load and renewables, thus allowing engineers to analyse several realistic cases corresponding to a specific time span. Specifically, the optimization code has been run considering different possible boundary conditions and the design of the system takes into account all these variations. In addition, the effect of the reference time span selected for the optimization process is studied and discussed. The MILP model also shows how the optimal output, thus the sizing of the system, can change according to the parameters involved in the process change, providing a complete tool that can be adapted to different applications and targets.

The paper is structured as follows: Section 2 presents the case study, the models of the various components related to the HRES and the MILP model as well. Section 3 shows the results of the simulations and Section 4 reports the conclusions of the work.

2. Research and Methods

2.1. Problem definition and goal of the work

Most of the works available in literature that deal with the optimal sizing of the HRESs provide results in a time span of 24 hours. They are based on the shapes of both load profile and energy production from renewables. In other works [35, 36], standard hours are selected with the aim of representing the whole dataset properly, thus providing results that can be compatible and extendable to the entire time period. This strategy is particular suitable to lower the computational efforts [37] in the calculation processes.

Sometimes, the daily fluctuations of the shapes of both load profile and renewable energy production do not allow engineers to choose a reference day or a significant time span to extend the results since they complicate the computation of the optimal system configuration, as well as the definition of the optimization strategy. In these cases, an assessment of the various optimal configurations, which depends on the dataset variability, is required in order to avoid a "wrong design" of the system that otherwise would not meet the real needs of the load.

The problem addressed in this paper regards the assessment of the optimal sizing of a HRES where the load profile, sun and wind curves present a high daily variability in a considered time period. An algorithm has been developed in order to analyse the daily configuration of the system, showing how the optimization results can be significantly affected by the variability of both load and renewable energies profiles. Firstly the developed model was run considering each day of a specific time period and then the whole month. The main benefit behind this methodology is the possibility of comparing and analysing several results. Moreover, it provides a general figure of the system behavior in the considered time period, as well as detailed information about the trend of both load and renewable energy sources per each day together with the system response.

The goal is to provide a tool capable of depicting various configurations of a HRES, thus helping engineers to assess and choose the size that best meets the energy demand using particular system requirements. The developed algorithm that has been used in the present case study is described in Subsection 2.2.

2.2. Case study

The algorithm has been applied to a case study of a mountain hut located at an altitude of $2,200\ m$ a.s.l., precisely at a latitude of $46.819°$ and a longitude of $11.442°$, in South-Tyrol (Italy) that is not connected with the national grid. The opening period of the hut is related to the summer season, namely from May to October, and its energy needs are satisfied through a diesel generator. The fuel consumption has been estimated to be about $15,000\ l$ per season, leading to an emission of CO_2 close to $10\ tons$. The power absorbed by the load can vary significantly in the daily hours and the days as well. Figure 1 shows the maximum, minimum and average power absorbed by the load per each hour of the day.

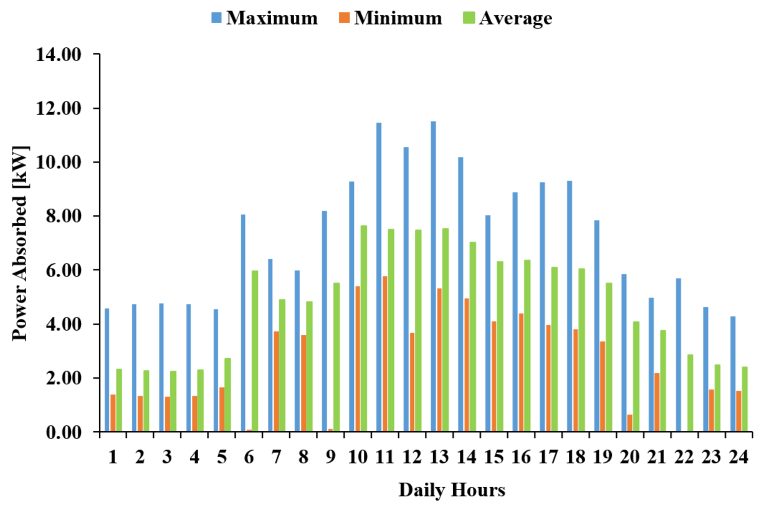

Figure 1: Maximum, minimum and average power absorbed by the load per day

The considered area is characterized by good sun and wind sources that could potentially supply all the energy needs to the hut. However, they are also outlined by a high variability that complicates the sizing of the system. The maximum, minimum and average recorded values of the Global Irradiance on the panel tilted surface (G), which is expressed in $[kWh/m^2]$, and the wind speed, which is expressed in $[m/s]$, are shown in Figures 2 and 3, respectively.

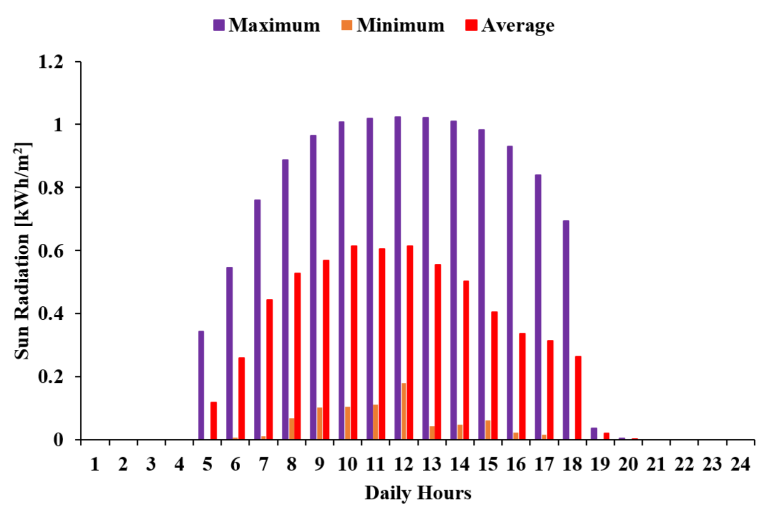

Figure 2: Maximum, minimum and average solar radiation per day

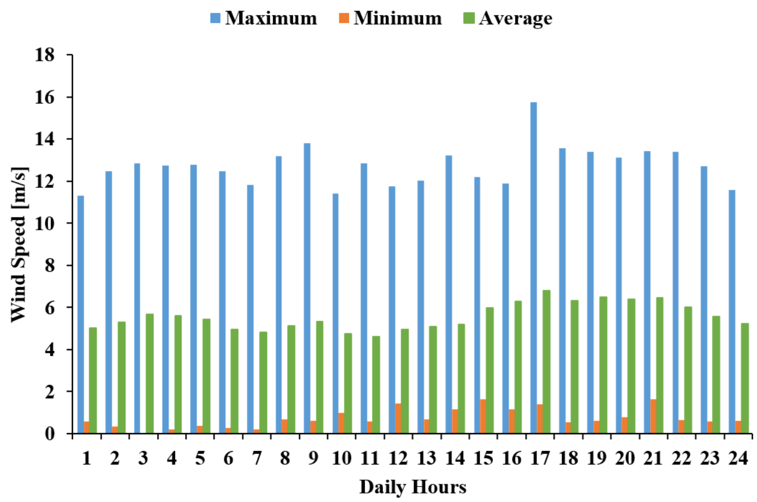

Figure 3: Maximum, minimum and average wind speed registered in the month of June

The data used to run the simulations have been collected through measurement campaigns and online tools. Precisely, the load profile and the wind speed were recorded in June 2018 through a power meter, which was installed in the main power line of the electrical control cabinet, and an anemometer. The month of June has been chosen since it is the one that presents the highest number of people in the hut. The data were recorded each minute in order to obtain, at the end of the measurements, the hourly averaged values of the absorbed power and wind speed. The global irradiance above the site in June 2018 were downloaded from the Photovoltaic Geographical Information System (PVGIS) [38]. It is worth noticing that the power generated, delivered or absorbed by the battery storage has been considered constant in each time interval: therefore, the produced power corresponds to the final energy production.

2.3. HRES components modeling

The location where the HRES will be installed is characterized by high solar and wind sources. Therefore, the HRES will be composed by PV panels, wind and a diesel generators coupled with the battery storage. Figure 4 shows the layout of the system. Sub-subsections 2.3.1, 2.3.2 and 2.3.3 describe the mathematical model of the PV system, wind turbines system and the diesel generator, respectively, while the one related to the battery storage is assessed in Sub-subsection 2.3.4.

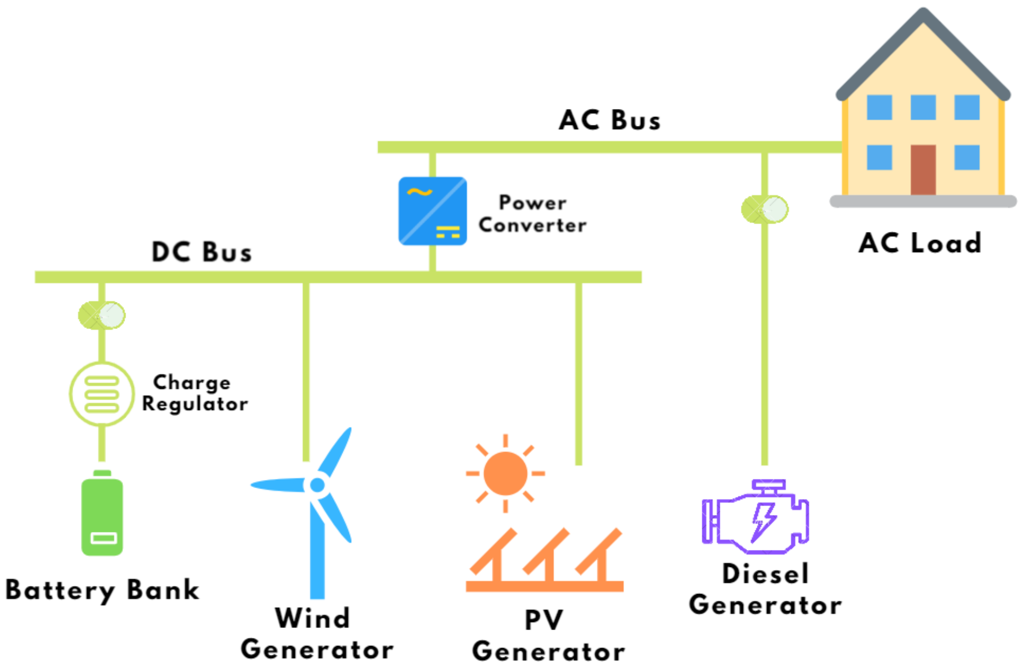

Figure 4: HRES layout

2.3.1. *PV system modeling*

The PV system has been modeled according to [39] considering a sharp poly-crystalline module [40], whose characteristics referring to Standard Test Conditions (STC) are listed in Table 1. The Direct Current DC power that is delivered by the PV system was computed through Eq. (1), where η_c is the cell efficiency, A_{eff} is the net cell opening area and G is the global irradiance on the panel tilted surface.

$$P_{PV-DC} = \eta_c A_{eff} G \tag{1}$$

In order to calculate the effective power delivered by the PV system, the losses related to the Balance Of System (BOS) were considered. These losses include several parameters that take into account the effective performance of the system components, such as the frequency converter, wirings, batteries, support racks and switches. The AC power delivered by the PV system is calculated through Eq. (2), considering the BOS efficiency η_{BOS} equal to 85%.

$$P_{PV-AC} = P_{PV-DC} \cdot \eta_{BOS} \tag{2}$$

Table 1: Characteristics of a sharp poly crystalline PV panel at STC

Parameter	Value	Unit of measure
Net cell opening area (A_{eff})	1.47	m^2
Cell efficiency at STC ($\eta_{n,c}$)	0.14	$-$
Power peak	240	W
Efficiency Loss Coefficient (β)	0.0044	°C^{-1}

In this model, the performance of the panels were evaluated under real operating conditions: in particular, the effect of the temperature and the solar radiation were considered for the evaluation of the cell efficiency η_c, as expressed by Eq. (3):

$$\eta_{\text{c}} = \eta_{\text{n,c}} \left[1 - \beta(T_{\text{C}} - 25) + 0.12\, log \frac{G}{1000} \right] \tag{3}$$

where $\eta_{n,c}$ is the rated efficiency of the cell in STC, β is the efficiency loss coefficient of the solar cell, with increasing temperature, expressed in [°C^{-1}], and T_C is the cell temperature. Along the same line, Eq. (4) evaluates T_C, where T_A is the ambient temperature, NOCT is the Nominal Operating Cell Temperature of the PV panel, τ is the transmissivity of the cell and α is the absorptivity.

$$T_{\text{C}} = T_{\text{A}} + \frac{G}{800}(NOCT - 20) \left(1 - \frac{\eta_{\text{c}}}{\tau\alpha} \right) \tag{4}$$

2.3.2. Wind turbine system modeling

The power produced by a wind turbine depends on the wind speed at the hub. Knowing the wind speeds, the produced power is obtained directly from the power curve of the turbine supplied by the manufacturer. Generally, the anemometers are located at a lower height than the hub one: therefore, Eq. (5) calculates the effective wind speed considering the most used formulation for heights lower than $150\,m$. Eq. (5) computes the values at different heights taking into account the surface roughness of the installation site, whose typical values are reported in [41].

$$w_{hub} = w_h \cdot \frac{ln\left(\frac{z_{hub}}{z_0}\right)}{ln\left(\frac{z_{anem}}{z_0}\right)} \tag{5}$$

Knowing the wind speeds at the hub height, the power output of a wind turbine is computed by means of its power curve. As described by Eq. (6), the wind turbine starts to generate power when the value of the wind speed reaches the cut-in one w_{cut-in}. The power output increases with the increasing wind speed until its rated value P_R is reached, corresponding to a wind speed w_R. Starting from w_R to the cut-out speed $w_{cut-out}$, the power output does not increase anymore, thus remaining constant and equal to P_R. Beyond the value of $w_{cut-out}$, the turbine stops to generate power to prevent failures. Then, the power curve of a possible wind turbine to be installed in the analysed site is shown in Figure 5.

$$P_{WT(STC)} = \begin{cases} 0, & \text{if } w_t < w_{cut-in} \text{ or } w_t > w_{cut-out} \\ P_i, & \text{if } w_{cut-in} \leq w_t < w_R \\ P_R, & \text{if } w_R \leq w_t \leq w_{cut-out} \end{cases} \tag{6}$$

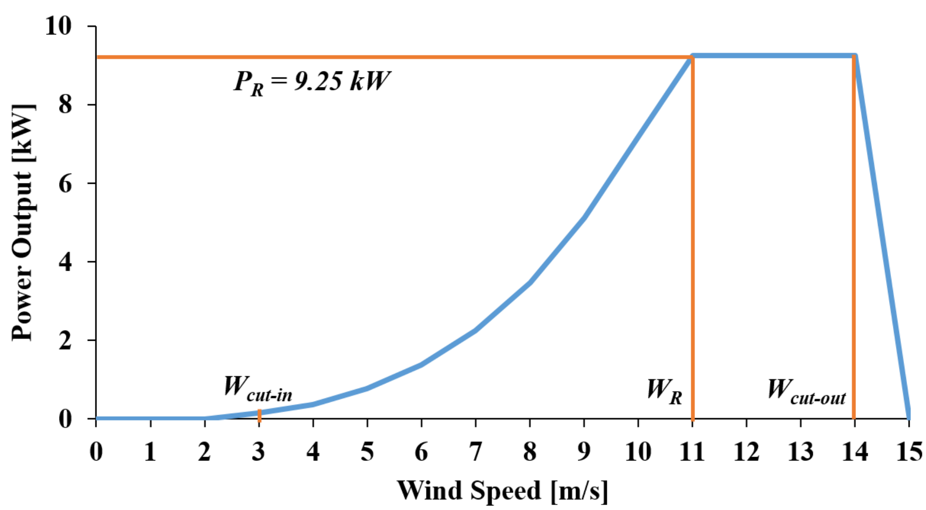

Figure 5: Possible power curve of a wind turbine eligible for the site of interest

It is worth noticing that the power output reported in Figure 5 considers an air density ρ of $1.225\ kg/m^3$ in STC (ρ_{STC}). In case of a different air density, Eq. (7) corrects the power output of the wind turbine P_{WT}. In this case study, an air density of $1.007\ kg/m^3$ has been considered [42].

$$P_{WT} = P_{WT(STC)} \cdot \frac{\rho_{air}}{\rho_{air(STC)}} \tag{7}$$

2.3.3. Diesel generator modeling

A diesel engine has been chosen as generator, which consists on a $3.5\ kW$ engine described in [43]. A greater size of the generator has not been chosen due to the implicit goal of maximizing the use of renewable energies. A larger generator would have added an additional constraint to limit the power output in determined cases. Certainly, this would have led to a better overall optimization, but also let the generator operate outside its best efficiency range, thus lowering the performance. The fuel consumption and the efficiency curves reported in [43] were used to model the power generated by the diesel engine. The fuel consumption of the generator is calculated with Eq. (8), which represents the fuel consumption curve of the engine fed by the diesel fuel. It depends on the generated electrical power P_{el} and a binary variable P_g that assumes the value of 0 or 1 whether the diesel generator is turned off or on, respectively. The coefficients ϕ and ψ have been obtained through laboratory tests and their respective values are equal to $0.087\ g/kW$ and 0.127.

$$F_C = \phi \cdot P_{el} + \psi \cdot P_g \tag{8}$$

Figure 6 shows the fuel consumption curve experimentally obtained in [43]. The fuel consumption is expressed in $[g/s]$ (Y-axis) as a function of the electrical power (X-axis), which is expressed in $[kW]$.

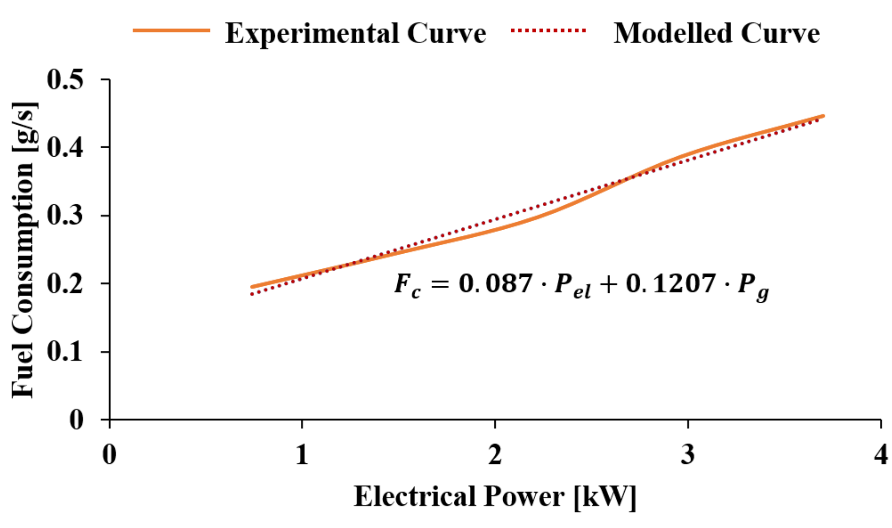

Figure 6: Fuel consumption curve of the diesel generator [43]

The efficiency of the diesel generator is calculated with Eq. (9), which corresponds to the ratio between the produced energy and the one provided by the fuel. The efficiency curve of the considered generator is shown in Figure 7.

$$\eta_{gen} = \frac{3.6 \cdot P_{el}}{\rho_{fuel} \cdot (F_C \cdot LHV_{fuel})} \tag{9}$$

LHV_{fuel} represents the Lower Heating Value (LHV) of the fuel and ρ_{fuel} is the fuel density equal to $42.6\ MJ/kg$ and $0.828\ kg/l$, respectively.

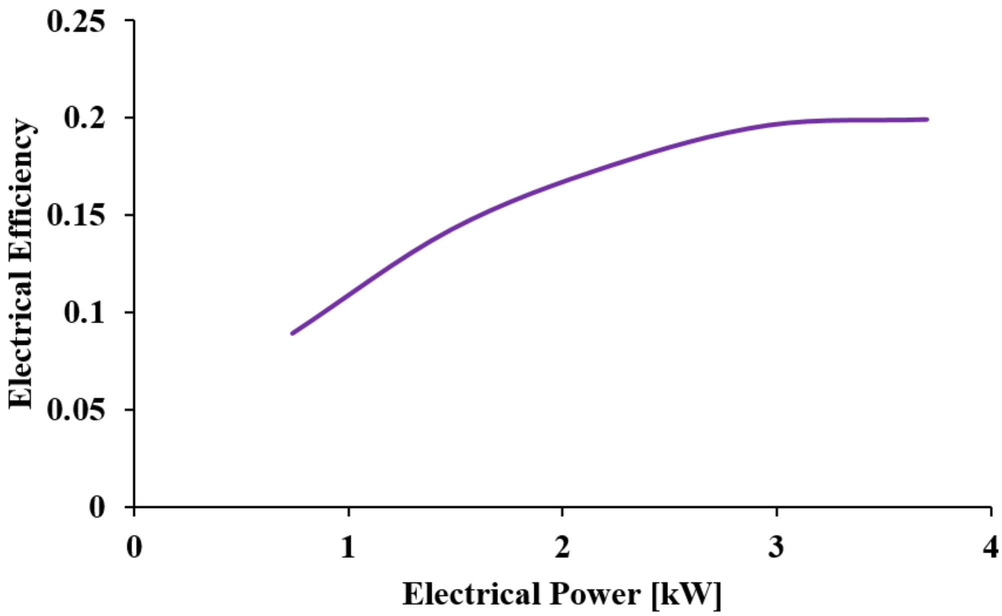

Figure 7: Efficiency curve of the diesel generator [43]

If a general motor is considered and the fuel consumption curve is not provided by the manufacturer, a simplified fuel consumption curve, which correlates the generator rated power to the generated electrical power, can be used [44].

2.3.4. Battery storage modeling

The battery storage in a HRES plays a key role since it stores the excess of energy produced by renewable sources, as well as to deliver it to the load during the high demand. Lead-acid batteries are chosen to model the storage. This type of battery is more suitable for climates subjected to low temperatures, which can be sometimes lower than 0 °C also in summer seasons, as it occurs in this case study. The energy that can be delivered or stored by the batteries at each time interval depends on the one that is already present in the battery E_{batt}, the self discharge rate σ and the energy balance between the generators and the load. During the discharging phases, the batteries supply the remaining energy to the load. This amount of energy is evaluated by means of Eq. (10). When the energy produced by the generators exceeds the load requirements, this overproduction can be stored in the batteries. The amount of the stored energy is expressed through Eq. (11).

$$\begin{aligned} E_{batt}(t) = E_{batt}(t-1) \cdot (1-\sigma) + [E_{Load}(t) \\ - (E_{PV}(t) + E_{WT}(t) + E_{Mot}(t))] \end{aligned} \tag{10}$$

$$\begin{aligned} E_{batt}(t) = E_{batt}(t-1) \cdot (1-\sigma) + [E_{PV}(t) \\ + E_{WT}(t) + E_{Mot}(t) - E_{Load}(t)] \end{aligned} \tag{11}$$

In order to simulate a real behavior of the batteries, the delivered energy cannot drop below the minimum State of Charge SOC_{min}, which is equal to the 20% of the batteries capacity B_C.

2.4. MILP modeling

The Linear Programming (LP) is an optimization algorithm in which a linear objective function has to be minimized or maximized with respect to a defined time period and a temporal discretization through time steps. When only some variables have to be integer, the problem is called Mixed Integer Linear Programming (MILP) [45]. A MILP problem consists of: i) an objective function, ii) decision variables and iii) constraints. The target of the MILP problem is to minimize an objective function choosing the best values of the decision variables that respect the established constraints. A flow chart that shows the MILP optimization steps is reported in Figure 8. Objective functions, decision variables and constraints that constitute the problem are described in Sub-subsections 2.4.1, 2.4.2 and 2.4.3, respectively.

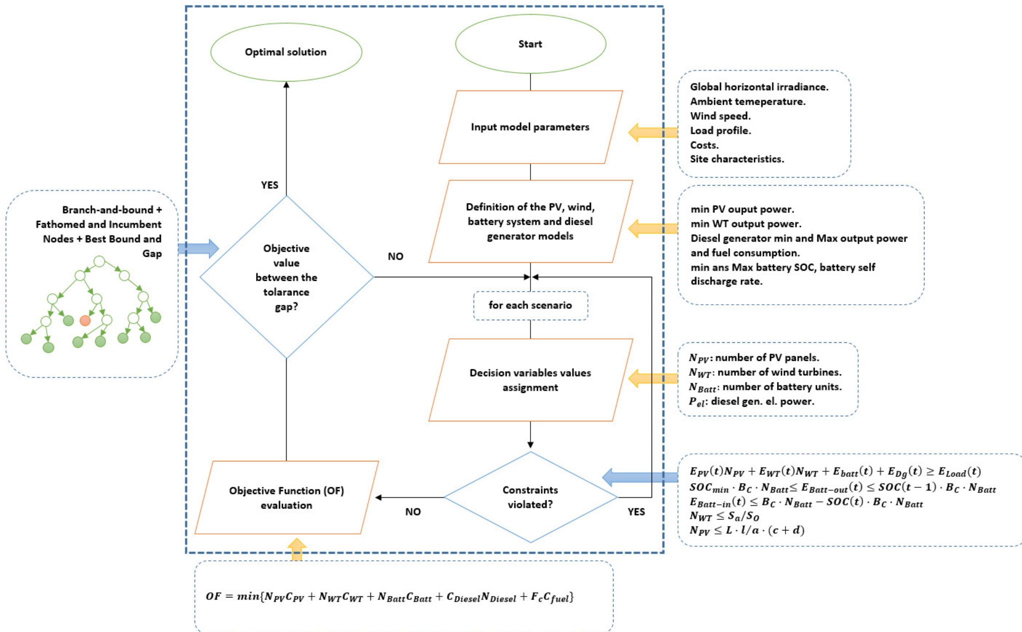

Figure 8: Flow chart of the MILP optimization algorithm

2.4.1. *Objective function*

The objective function of the MILP algorithm is the total Net Present Cost (NPC) of the system, which is the sum of the total NPC related to each element that constitutes a HRES. The total cost of an element embedded in a HRES can be defined as the sum of the initial capital cost C_{IN}, the operation and maintenance (O&C) cost $C_{O\&M}$ and the replacement one C_R. If the fuel is consumed, the supposed quantity of the fuel consumption in the lifetime of the generator F_c and its cost C_{fuel} must be included. In order to obtain the NPC, all the costs must be actualized at the present stage of the project. The objective function is expressed by Eq. (12).

$$min\,(N_{PV}C_{PV} + N_{WT}C_{WT} + N_{Batt}C_{Batt} + C_{Diesel}N_{Diesel} + F_cC_{fuel}) \tag{12}$$

where N_{PV}, N_{WT} and N_{Batt} are the total number of PV panels, wind turbines and batteries units, respectively. N_{Diesel} is the number of diesel generators that in this case has been set equal to 1 and does not constitute a decision variable of this specific optimization problem. Nevertheless, it has been included in the problem in order to improve the flexibility of the algorithm when a different case study is used. C_{PV}, C_{WT}, C_{Batt} and C_{Diesel} are the total NPCs of a single PV panel, wind turbine, battery and diesel generator respectively. F_c and C_{fuel} are the fuel consumption of the diesel generator and the fuel cost, respectively.

2.4.2. Decision variables

The decision variables determine the output of the objective function. The target of the MILP algorithm consists on minimizing the objective function, thus to find the values of the decision variables for reaching this target. In the analysed case, the decision variables are the following:

- N_{PV}: number of PV panels;
- N_{WT}: number of wind turbines;
- N_{Batt}: number of batteries units;
- $E_{Batt}(t)$: energy delivered or absorbed by the battery per each time interval;
- $E_{Dg}(t)$: energy delivered by the diesel generator per each time interval.

2.4.3. Constraints

The constraints are mathematically expressed in form of equalities and inequalities, thus limiting the values that can be attributed by the algorithm to the decision variables. They are related to technological, economic or geometrical limitations. In this case study, technological and geometrical constraints are involved. Eq.s (13), (14) and (15) set the technological constraints, while Eq.s (16), (18) and (17) define the geometrical ones. Eq. (13) expresses the balance between the energy produced by the HRES and the load demand. The produced energy has to satisfy the load demand per each time interval. It is also assumed that the excess of the produced energy can be managed by the inverter connected to the PV modules and the pitch control system of the wind turbines, thus reducing the power output by letting the generators operate in off-design conditions according to the power curves of the machines.

$$E_{Load}(t) \leq E_{PV}(t)N_{PV} + E_{WT}(t)N_{WT} + E_{Dg}(t) + E_{Batt}(t) \tag{13}$$

Eq.s (14) and (15) limit the energy that can be delivered or absorbed by the battery storage per each time interval. Eq. (14) sets both lower and upper limits of the energy delivered by the batteries per each time interval, thus establishing that the energy delivered by the batteries cannot be lower than the minimum State Of Charge (SOC_{min}), which corresponds to 20% of the battery capacity (B_C). In addition, the maximum energy delivered per each time interval cannot exceed the SOC of the batteries, i.e. the effective amount of energy left in the batteries after their operation in the previous time interval.

$$SOC_{min} \cdot B_C \cdot N_{Batt} \leq E_{Batt-out}(t) \leq SOC(t-1) \cdot B_C \cdot N_{Batt} \quad (14)$$
$$E_{Batt-in}(t) \leq B_C \cdot N_{Batt} - SOC(t) \cdot B_C \cdot N_{Batt} \quad (15)$$

Eq. (16) limits the available ground area of the wind turbines in the installation site: precisely, S_o is the one occupied by a wind turbine. It is worth noticing that the total area that can be occupied by the wind turbines $N_{WT} \cdot S_o$ cannot exceed the available area S_a.

$$N_{WT} \leq \frac{S_a}{S_o} \quad (16)$$

Eq. (17) limits the ground area that can be occupied by PV panels: namely, L and l are the larger and the smaller sides of the available ground area, respectively, a is the smaller side of the PV module, c is the projection of the larger side b of the panel on the ground and d is the distance between the rows of the PV panels. A clear description of these geometrical parameters is shown in Figure 9.

$$N_{PV} \leq \frac{L \cdot l}{a \cdot (c+d)} \quad (17)$$

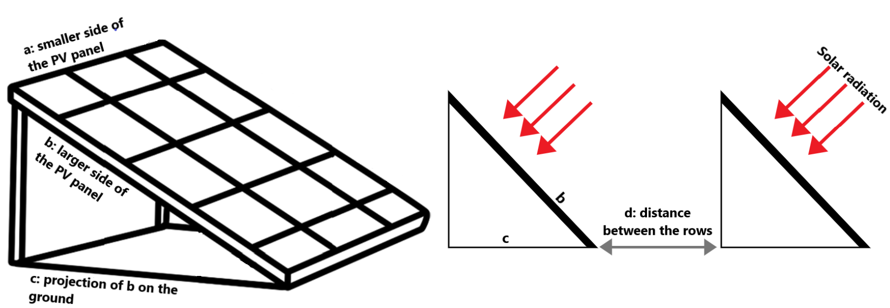

Figure 9: Dimensions of the PV panels

Eq. (18) reports the calculation process used to obtain the constraints deriving by Eq. (17).

$$\begin{cases} N_{PV} \leq \frac{l}{a} \cdot N_{rows} \\ N_{rows} = \frac{L}{c+d} \\ c = b \cdot cos(\beta) \\ d = k \cdot sin(\beta) \\ k = \frac{1}{tan(61^{\circ} - Latitude)} \end{cases} \tag{18}$$

where β is the tilt angle of the PV panel, b is the larger side of the PV module and k is a coefficient used to calculate the distance between two PV panels rows, which depends on the latitude where they are installed. Table 2 lists the values of the parameters used to limit the ground areas occupied by the PV panels and the wind turbines.

Table 2: Parameters adopted to limit the ground areas of PV panels and wind turbines

Parameter	**Value**	**Unit of measure**
S_a	100	m^2
S_o	25	m^2
L	10	m
l	10	m
a	0.994	m
b	1.652	m
β	30	$degrees$
$Latitude$	46.819	$degrees$

2.5. Economic analysis - NPC of the HRES

The MILP algorithm computes the optimal solution of the problem finding the values of the optimization variables that minimize the objective function, which is the minimum NPC of the system. Generally, the NPC of an investment allows the investors to choose the optimal option among different ones. The NPC is defined as the sum of the present value of all the costs minus the sum of the present value of all the benefits. Therefore, the NPC of a component considers its total cost that is composed by the initial capital cost C_{IN}, the operation and maintenance (O&M) cost $C_{O\&M}$, the replacement cost C_R and, eventually, the fuel cost C_{fuel} taking into account the Time Value of Money (TVM) through a discount factor D_f. For sense of clarity, D_f is used to calculate the present value of the cash flow during the project lifetime and it is defined by Eq. (19).

$$D_f = \frac{1}{(1+i)^n} \tag{19}$$

Referring to Eq. (19), i is the real discount rate, which takes into account the money inflation as defined by Eq. (20), and n is the lifetime of the project expressed in years.

$$i = \frac{i_{nom} - f}{1+f} \tag{20}$$

Referring to Eq. (20), i_{nom} represents the nominal discount rate that indicates the rate at which money can be borrowed, while f is the expected inflation rate. D_f decreases over the years, thus stating that a future cash flow is less worth than a present one. Considering an expected inflation rate of about 2%, D_f has been considered equal to 6%.

3. Results and comments

The goal of the work is to demonstrate that the choice of the dataset used to run the simulation has a crucial role on the results: therefore, all the outcomes of the calculations require a correct evaluation to avoid misunderstandings. In particular, simulations aim to show how the optimal solution varies depending on the assumptions made on the renewable energy sources profiles. The MILP optimization algorithm was used taking into account three different cases related to the HRES:

- **Case** 1: The simulation was run considering a time span of 24 hours. In this case, it is possible to analyse how the configuration of the HRES changes depending on the fluctuations of the power absorbed by the load and the power produced by the renewable sources as well. This case is important for analysing how the variability of the dataset can affect the optimal solution. The reduction of the Greenhouse gases (GHGs) emissions derived by feeding the load with the HRES instead of only a diesel generator is also shown.

- **Case** 2: The simulation was run considering a time span of 1 month. In this case, the output of the analysis is a unique configuration that meets the constraints per each hour of the month, thus satisfying the load requirements. Furthermore, it is the most robust solution, but also the most expensive. Indeed, the system will be oversized and the excess of the produced energy will be managed by the PV inverter and the pitch control system of the wind turbines that can shift the operating point of PV panels and wind turbines, respectively, to off-design conditions accordingly to the required power output regulation. Also in this case, a reduction of GHGs emissions is presented.

- **Case** 3: The simulation was run considering a time span of 24 hours, varying the constraint of the load requirements from 100% of the actual value to 50%, with steps of 10%. Indeed, it can be supposed that it is not always necessary to satisfy the total hourly load described by the load profile curves, applying a demand side management strategy. In these cases, a percentage of the load can be sometimes sacrificed since it is not essential. For instance, loads like a cold storage can hold some hours without the electrical supply. This case aims at demonstrating that a reduced percentage of the load requirements lowers the dependency on the renewable energy sources profiles, thus reducing the variability of the total NPC between the most expensive and the cheapest solutions. As a result, the algorithm helps engineers to reduce the total cost of the system, adopting a configuration that is not oversized over the entire time period. Furthermore, a sensitivity analysis has been performed in order to assess the effects of fuel and battery prices variations. Simulations have been run considering a fuel price variation from 1.4 €$/l$ to 3.8 €$/l$, with steps of 0.2 €$/l$, and a decreasing battery price with steps of 5% until the 50% of its actual cost per kWh is reached. This wide fuel price variation has been chosen to better point out how the fuel price variation affects the HRES optimal sizing. For sense of clarity, diesel prices can vary from 1.4 €$/l$ in developing countries to 3 €$/l$ in remote areas characterized by a complicate fuel distribution system [46] and [47].

Per each case, an economic analysis based on the NPC has been carried out. The economic parameters used in the simulation are described in Table 3.

Table 3: Economic parameters used to run the simulation [44, 48, 49, 50, 51]

PV panels	C_{IN}	$1,400$	$€/kW$
	$C_{O\&M}$	0.081	$€/kW(daily)$
Wind turbines	C_{IN}	$2,000$	$€/kW$
	$C_{O\&M}$	0.095	$€/kW(daily)$
Batteries	C_{IN}	$1,223$	$€/kWh$
	$C_{O\&M}$	0.1	$€/kWh(daily)$
	C_R	612	$€/kWh$
Diesel generator	C_{IN}	550	$€/kW$
	$C_{O\&M}$	438	$€/year$
	C_{fuel}	2	$€/l$

3.1. Case 1 and case 2

Results of the first two cases are presented in Table 4. The MILP algorithm computes the optimal number of PV panels, wind turbines and battery units that minimizes the total NPC of the system per each day related to the considered time interval. The algorithm also computes the value of the energy delivered or absorbed by the batteries, thus optimizing the energy produced by the generators and minimizing the effect of the fluctuating renewable energy sources.

Table 4 lists the results obtained in Cases 1 and 2, showing that the optimal size of the system varies over the considered days and highlighting a noticeable difference between the solution characterized by the highest and the lowest NPC.

Results also show that the variability of the power absorbed by the load and the fluctuating nature of both sun radiation and wind speed strongly affects the output of the simulation. Moreover, it can be noticed how the results of the simulation change according to the considered time span. When considering a time span of 24 hours, the algorithm sizes the system in order to optimize the energy produced by renewable energy sources, reducing the fuel consumption of the diesel generator and considering also the energy stored in the battery storage during the night hours when the sun radiation cannot contribute to the energy supply. As a consequence, the battery storage is completely discharged at the end of the day, contributing to a lower sizing and, eventually, to the impossibility of meeting the power demand if the first hours of the following day are characterized by low values of wind speeds. The simulation over the time span of the entire month (Case 2), as shown in the last line of Table 4, considers the worst scenario in which there is a lack of both solar and wind production in the different days: therefore, the result presents a bigger capacity of the battery storage. Figures 10 and 11 show the simulation results considering the time period of the 7^{th} and the 17^{th} of June 2018, respectively. These two days were selected in order to highlight the behavior of the system when dealing with a different load and with variable profiles of the sun radiation and the wind speed. It is worth noticing that the negative values in the battery power profile indicate the periods of the day during which the battery is charged, while the positive values refer to the supply of power from the battery, namely the discharge phase. In the first case, the optimal solution computed by the algorithm does not include the wind turbines due to the lack of the wind source. The algorithm computes the optimal solution relying significantly on the contribution of the diesel generator during the daily hours characterized by a lack of the sun source. In the second case, the optimal solution computed by the optimization algorithm includes the exploitation of the wind source and a minimum contribution of the diesel generator is required. In this case, the HRES is able to satisfy the load requirements relying almost entirely on renewable energy generators and batteries. In both cases, it can be noticed how the PV production and the batteries operations are complementary. The system aims to charge the batteries with the excess of PV production to use them when renewable resources cannot be exploited. For sense of clarity, it is worth noticing that the trend of the energy supplied by the PV system does not correspond exactly to the one reported in Figure 2 since a control system is implemented to modulate the power delivered through the solar inverter. Similarly, the wind turbine includes a pitch control functionality to modulate the generated power when an excessive power production is achieved. Figure 12 shows the trend of the load profile, the energy produced by the HRES and the SOC of the batteries in the entire month. It is worth noticing that the diesel generator operates when the energy cannot be supplied by both PV panels and wind turbines, thus operating at its rated power to optimize the fuel consumption. The diesel generator does not operate when solar and wind sources are abundant. In this case, the entire energy needs are supplied by PV panels, the wind turbine and the battery storage, either supplying energy when needed or absorbing its overproduction. It can be also appreciated how a change of the simulation time span from 24 hours to the entire month affects the simulation results related to each single day computed in a scenario of 24 hours. For instance, considering the 7^{th} of June, the optimization algorithm has to compute the charge/discharge operation of the battery pack and the power delivered by the diesel generator in a day taking into account the previous operating conditions and the state of the

HRES. Therefore, results shown in Figures 10 and 12 differ one to each other.

Table 4: Comparison between different configurations of the HRES. Case 1 (results of each single day) and Case 2 (results of the whole month)

Day	N_{PV}	N_{WT}	Battery [kWh]	NPC_{TOT} [€]	NPC_{PV} [€]	NPC_{WT} [€]	NPC_{Bat} [€]	NPC_{Mot} [€]
1st June	103	0	12	169,720	44,523	0	35,573	89,624
2nd June	119	0	20	152,967	51,439	0	59,288	42,240
3rd June	138	0	16	167,448	59,652	0	47,430	60,366
4th June	169	0	21	151,011	73,052	0	62,252	15,706
5th June	146	0	21	148,444	63,110	0	62,252	23,082
6th June	89	0	17	103,946	38,471	0	50,395	15,080
7th June	63	0	8	122,607	27,232	0	23,715	71,659
8th June	93	0	12	147,277	40,200	0	35,573	71,504
9th June	182	0	17	182,475	78,672	0	50,395	53,409
10th June	74	0	8	98,311	31,987	0	23,15	42,608
11th June	1	2	15	175,084	432	49,397	44,466	80,788
12th June	72	0	8	125,813	31,123	0	23,715	70,975
13th June	50	1	7	92,858	21,613	24,699	20,751	25,796
14th June	105	0	17	176,568	45,387	0	50,395	80,786
15th June	75	1	4	94,895	32,420	24,699	11,858	25,919
16th June	189	1	13	160,185	81,697	24,699	38,537	15,251
17th June	126	1	14	137,282	54,465	24,699	41,502	16,617
18th June	73	1	5	86,342	31,555	24,699	14,822	15,266
19th June	29	2	6	94,260	12,536	49,397	17,786	14,541
20th June	60	0	22	150,473	25,936	0	65,217	59,321
21st June	77	0	24	120,933	33,284	0	71,145	16,504
22nd June	48	1	6	97,159	20,749	24,699	17,786	33,926
23rd June	57	0	16	115,275	24,639	0	47,430	43,206
24th June	74	0	18	129,388	31,987	0	53,359	44,041
25th June	46	2	18	130,500	19,884	49,397	53,359	7,860
26th June	49	2	4	115,954	21,181	49,397	11,858	33,518
27th June	35	1	0	47,688	15,129	24,699	0	7,860
28th June	26	1	4	82,272	11,239	24,699	11,858	34,477
29th June	27	2	3	84,371	11,671	49,397	8,893	14,409
30th June	106	2	23	171,258	45,820	49,397	68,181	7,860
Month	110	1	10	171,473	47,549	24,699	29,644	69,851

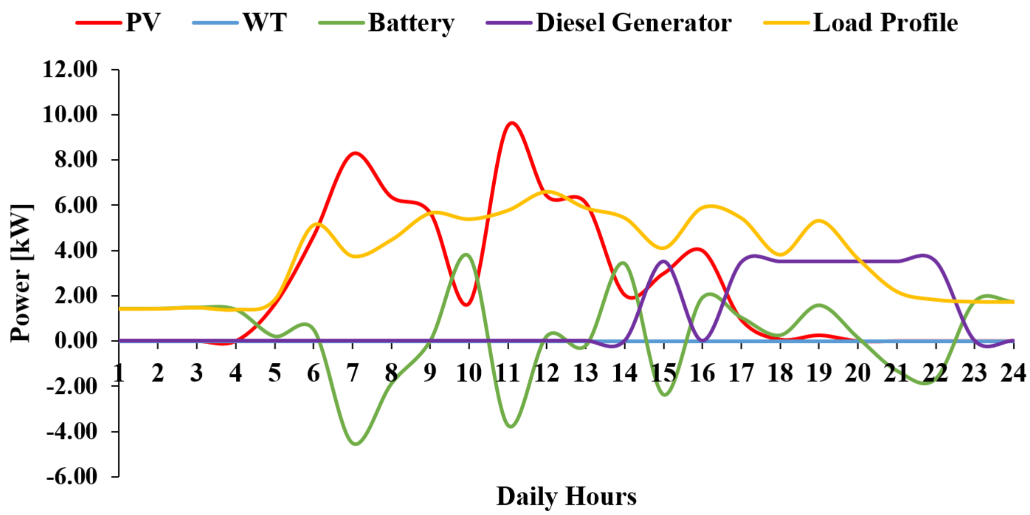

Figure 10: Simulation results of the 7th June 2018

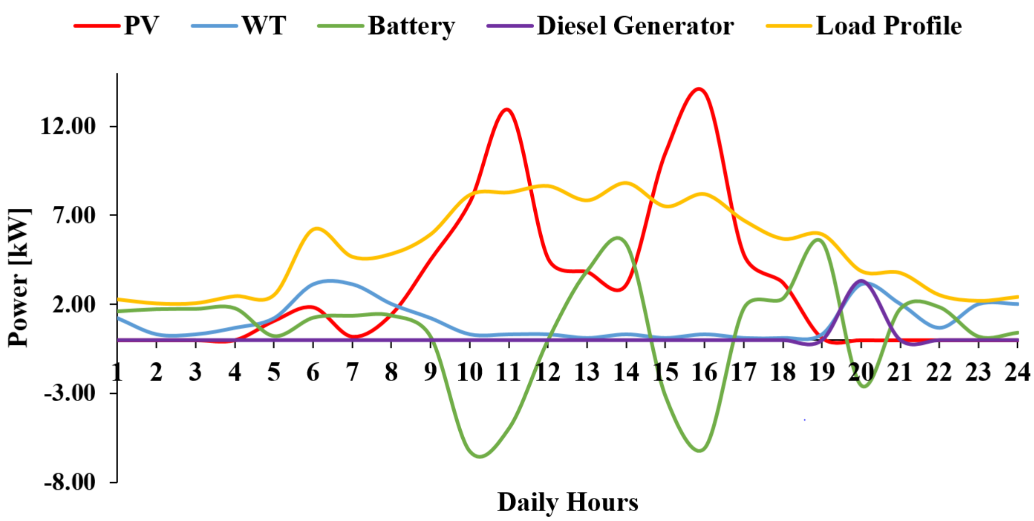

Figure 11: Simulation results of the 17th June 2018

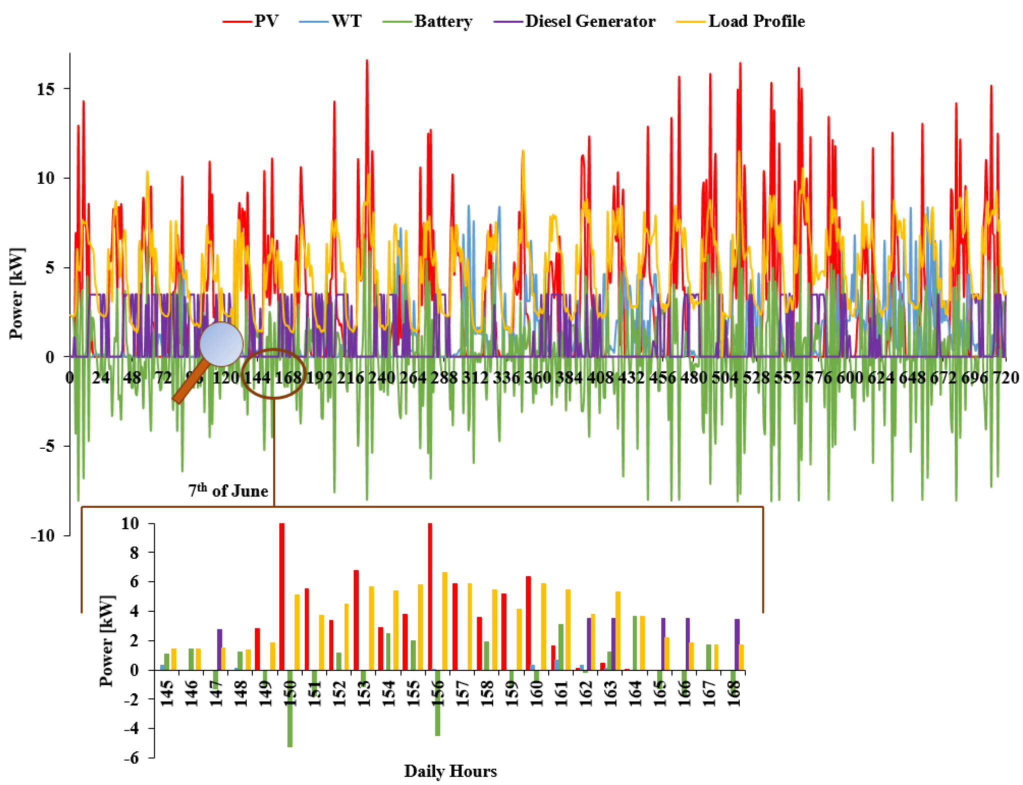

Figure 12: Load profile and contribution of the HRES over a month

Table 5 shows the GHGs emissions in terms of CO_2 and NO_x due to the electrical energy provided by the diesel generator. It also provides a comparison between the total GHGs emissions if the load would be entirely satisfied by the diesel generator. It is worth noticing the remarkable reduction due to the introduction of the renewable energy technologies in the energy system.

Table 5: GHGs emissions savings

Day	El. Energy Delivered [kWh]	CO_2 [kg]	NO_x [kg]	CO_2 diesel only [kg]	NO_x diesel only [kg]	CO_2 savings %	NO_x savings %
1st June	31.3	71	0.38	33	1.74	79	79
2nd June	12.9	32.2	0.17	330	1.72	90	90
3rd June	19.8	48	0.25	332	1.73	86	85
4th June	2.8	8.3	0.04	307	1.59	97	97
5th June	5.4	16.4	0.09	296	1.53	94	94
6th June	2.5	8.5	0.04	284	1.48	97	97
7th June	24.5	55.2	0.29	297	1.53	81	81
8th June	24.4	55.2	0.29	293	1.52	81	81
9th June	17.5	39.4	0.21	324	1.68	88	88
10th June	13.1	32.1	0.17	369	1.91	91	91
11th June	28	63.1	0.34	301	1.56	79	79
12th June	24.1	55.4	0.29	319	1.65	83	82
13th June	6.8	15.8	0.08	310	1.61	95	95
14th June	28	63.1	0.34	294	1.53	79	78
15th June	6.9	15.8	0.08	336	1.75	95	95
16th June	2.6	8.4	0.04	340	1.77	98	98
17th June	3.3	8	0.04	364	1.89	98	98
18th June	2.6	8.4	0.04	364	1.90	98	98
19th June	2.2	8.6	0.04	337	1.76	97	98
20th June	19.2	48.3	0.25	345	1.80	86	86
21st June	3.2	8	0.04	343	1.79	98	98
22nd June	9.8	24.1	0.13	367	1.91	93	98
23rd June	13.4	31.9	0.17	364	1.90	91	91
24th June	13.8	31.6	0.17	398	2.08	92	92
25th June	0	0	0	386	2.02	100	100
26th June	9.6	24.2	0.13	340	1.77	93	93
27th June	0	0	0	356	1.86	100	100
28th June	10.1	23.9	0.13	350	1.83	93	93
29th June	2.1	8.6	0.04	376	1.96	98	98
30th June	0	0	0	385	2.01	100	100
Month	678	1,710	25	10,138	52.8	83	52

3.2. Case 3

Table 6 refers to Case 3 and provides the values of the minimum and the maximum NPC, as well as the difference between them whether a hourly energy deficit is accepted. It is worth noticing that, reducing the percentage of the total hourly load, the difference between the maximum and the minimum NPC decreases down to 57%.

Table 6: Minimum and maximum NPCs from different configurations with demand management

% of load demand to satisfy	**Min NPC [€]**	**Max NPC [€]**	**Max - Min NPC [€]**	**% of the decrease**
100%	$47,688$	$182,475$	$134,787$	–
90%	$44,662$	$165,088$	$120,426$	11 %
80%	$42,501$	$147,645$	$105,144$	22 %
70%	$40,339$	$130,639$	$90,300$	33 %
60%	$38,178$	$113,005$	$74,827$	44 %
50%	$37,252$	$95,863$	$58,611$	57 %

Table 7 lists the results obtained in a time span of 24 hours, considering a decreasing battery price with steps of 5% until a drop of 50% is achieved, corresponding to a battery price of 581 €$/kWh$. Table 7 highlights how a reduction of the battery price affects the number of PV panels, wind turbines, battery units and the NPCs of both HRES and diesel generator. It can be noticed how a reduction of the battery price leads to an increase of the battery units until their price drops to 50%. Precisely, the most expensive solution occurs for the simulation of the 16^{th} of June, while the cheapest is obtained for the 9^{th} of June. The need to exploit the sun source, coupled with a consistent reduction of the battery price, leads to an increase of the PV units so that the battery cost becomes competitive with respect to the PV one. Considering the diesel generator, its total NPC slightly increases when the battery price decreases of 10%, which corresponds to $1,040$ €$/kWh$, since the generator is preferred than the PV panels: for this reason, the cost of the diesel generator decreases until to $7,860$ € since it is only used as a backup.

Table 7: Results obtained considering a decreasing battery price

Battery Price [€/kWh]	**PV panels Max | Min**	**Wind turbines Max | Min**	**Battery units Max | Min**	**NPC Generator [€] Max | Min**	**NPC HRES [€] Max | Min**
1,223	182 | 35	0 | 1	17 | 0	53,409 | 7,860	182,475 | 47,688
1,162	182 | 35	0 | 1	17 | 0	53,409 | 7,860	179,962 | 47,688
1,101	151 | 35	0 | 1	22 | 0	53,432 | 7,860	177,415 | 47,688
1,040	145 | 29	0 | 1	23 | 1	53,389 | 7,860	174,045 | 47,615
978	145 | 29	0 | 1	23 | 1	53,389 | 7,860	170,589 | 47,465
917	141 | 29	0 | 1	24 | 1	52,862 | 7,860	167,155 | 47,317
856	142 | 29	0 | 1	41 | 1	16,800 | 7,860	163,329 | 47,169
755	144 | 29	0 | 1	45 | 1	7,860 | 7,860	142,457 | 46,924
697	144 | 25	0 | 1	45 | 2	7,860 | 7,860	146,130 | 46,744
639	144 | 25	0 | 1	45 | 2	7,860 | 7,860	139,804 | 46,463
581	205 | 25	0 | 1	29 | 2	7,860 | 7,860	137,314 | 46,182

Table 8 shows the results obtained after a sensitivity analysis performed on the diesel price, considering the most expensive and the cheapest system configuration. An increasing diesel price with steps of 0.2 €$/l$ has been considered, starting from a value of 1.4 €$/l$ to a value of 3.8€$/l$. When dealing with the most expensive solution, an increase of the diesel price from 1.4 to 1.6 €$/l$ leads to a consistent increase of the number of PV panels and battery units. Then, their number remains stable until a value of 2.4 €$/l$ is reached. This occurs in the day characterized by the most expensive configuration changes from the 9^{th} to the 14^{th} of June during which the HRES configuration is the same also with a diesel price of 2.8 €$/l$. This is due to the fact that, considering a diesel price that varies from 1.6 €$/l$ to 2.8 €$/l$, the increase does not affect the competitiveness of the diesel generator with respect to the other generators. This is also demonstrated by the fact that the total NPC of the system grows progressively. Moving from 2.8 €$/l$ to 3 €$/l$, the algorithm favors a solution constituted by a higher number of battery units and the diesel generator, where the former does not contribute to the load energy needs. This is demonstrated by the fact that the total NPC of the system remains constant.

Table 8: Simulation results with a decreasing fuel price

Fuel Price [**€/l**]	**PV panels** **Max** | **Min**	**Wind turbines** **Max** | **Min**	**Battery units** **Max** | **Min**	**NPC HRES** [**€**] **Max** | **Min**	**Day of June** **Max** | **Min**
1.4	169 | 35	0 | 1	6 | 0	167,261 | 47,688	9^{th} | 27^{th}
1.6	182 | 35	0 | 1	17 | 0	173,365 | 47,688	9^{th} | 27^{th}
1.8	182 | 35	0 | 1	17 | 0	177,920 | 47,688	9^{th} | 27^{th}
2.0	182 | 35	0 | 1	17 | 0	182,475 | 47,688	9^{th} | 27^{th}
2.2	182 | 35	0 | 1	17 | 0	187,030 | 47,688	9^{th} | 27^{th}
2.4	182 | 35	0 | 1	17 | 0	191,585 | 47,688	9^{th} | 27^{th}
2.6	105 | 35	0 | 1	17 | 0	198,445 | 47,688	14^{th} | 27^{th}
2.8	105 | 35	0 | 1	17 | 0	205,738 | 47,688	14^{th} | 27^{th}
3.0	105 | 35	0 | 1	52 | 0	207,396 | 47,688	14^{th} | 27^{th}
3.2	105 | 35	0 | 1	52 | 0	207,396 | 47,688	14^{th} | 27^{th}
3.4	105 | 35	0 | 1	52 | 0	207,396 | 47,688	14^{th} | 27^{th}
3.6	105 | 35	0 | 1	52 | 0	207,396 | 47,688	14^{th} | 27^{th}
3.8	205 | 35	0 | 1	52 | 0	207,396 | 47,688	14^{th} | 27^{th}

4. Conclusions

A MILP algorithm has been developed with the aim of analysing how the choice of the reference dataset for designing a HRES can strongly affect the optimal configuration due to the strong variability of the renewable energy sources. The algorithm was used considering a case study of a mountain hut located in South-Tyrol (Italy) at an altitude of $2,200$ m a.s.l. where the national power grid is not present. The applied methodology considers a hybrid system composed by PV panels, wind turbines, a diesel generator and lead-acid batteries as storage solution.

The algorithm computes the optimal number of PV panels, wind turbines, battery units and the energy provided by the diesel generator, constituting the optimization variables of the problem, with the aim of minimizing the total Net Present Cost (NPC) of the system over its entire lifetime. As input, a dataset based on a measurement campaign performed in the month of June 2018 related to the wind speed on site and the power consumption of the hut was used. These data were collected each minute per each day and their hourly average values were computed and used. The data related to the sun radiation were downloaded by the PVGIS database. Two sizing approaches were evaluated: in one case, the sizing of the components is based on the dataset of single days operation; alternatively, the sizing is based on the whole dataset covering one month operation.

Based on these two approaches, the algorithm simulates the behavior of the optimal system over one month.

Results showed a strong variability related to the optimal sizing of power generators and batteries in the HRES, which strongly depends on the variability of the renewable sources as well as on the load profile. This demonstrates that the proper selection and analysis of the dataset for sizing a HRES is fundamental to obtain adequate performance. Considering only a daily load profile and a daily pattern of both sun and wind sources, the HRES sizing could not meet the needs of the load in all the days if a proper representative day of the entire month is not defined. However, a lower capital cost would be required in most of the cases. On the other hand, its sizing leads to an oversizing of the components when dealing with the whole dataset. Therefore, a demand management could help to reduce the size of the components and, at the same time, grate the energy supply when the most demanding conditions occur. Results showed that: 1. the optimal sizing of a HRES strongly depends on the renewable sources and their variability, 2. the storage systems, coupled with conventional generators, are still necessary to avoid the oversizing of the entire system, as well as of the batteries bank, 3. the modulation of PV power, wind power and an eventual demand side management strategy is crucial to avoid the oversizing due to the variable percentage of the load to be satisfied each hour of the day, which decreases the difference between the maximum and the minimum costs of the HRES . Results also demonstrate a significant reduction of the GHGs emissions due to the use of renewable energy technologies. Furthermore, a sensitivity analysis has been performed on both the fuel and battery costs, showing how these parameters can influence the optimal sizing of the system. In particular, considering a possible future scenario characterized by a significant battery price reduction, HRESs would significantly reduce their dependency on fossil-fuel conventional generators.

This algorithm constitutes a tool capable of providing a detailed description of different possible scenarios, thus helping engineers to design the system properly. Further developments of this investigation may include the use of a PHES equipped with Pumps-as-Turbines (PaTs) instead of conventional hydraulic turbines or conventional batteries storage systems. Indeed, the lower cost of PaTs compared to conventional hydraulic turbines and battery storage systems can reduce the total cost of an HRES, thus pushing further their future deployment.

References

[1] J. M. Dyrstad, A. Skonhoft, M. Q. Christensen, E. T. Ødegaard, Does economic growth eat up environmental improvements? Electricity production and fossil fuel emission in OECD countries 1980–2014, Energy Policy 125 (2019) 103–109. doi:https://doi.org/10.1016/j.enpol.2018.10.051.

[2] E. A. Feilat, S. Azzam, A. Al-Salaymeh, Impact of large PV and wind power plants on voltage and frequency stability of Jordan's national grid, Sustainable Cities and Society 36 (2018) 257–271. doi:https://doi.org/10.1016/j.scs.2017.10.035.

[3] C. Li, H. Shi, Y. Cao, J. Wang, Y. Kuang, Y. Tan, J. Wei, Comprehensive review of renewable energy curtailment and avoidance: A specific example in china, Renewable and Sustainable Energy Reviews 41 (2015) 1067–1079. doi:https://doi.org/10.1016/j.rser.2014.09.009.

[4] V. Gambino, R. Del-Citto, P. Cherubini, C. Tacconelli, A. Micangeli, R. Giglioli, Methodology for the Energy Need Assessment to Effectively Design and Deploy Mini-Grids for Rural Electrification, Energies 12(3) (2019) 574. doi:https://doi.org/10.3390/en12030574.

[5] A. H. Fathima, K. Palanisamy, Optimization in micro grids with hybrid energy systems – A review, Renewable and Sustainable Energy Reviews 45 (2015) 431–446. doi:https://doi.org/10.1016/j.rser.2015.01.059.

[6] L. P. Amaral, A. Araújo, E. Mendes, N. Martins, Economic and environmental assessment of renewable energy micro-systems in a developing country, Sustainable Energy Technologies and Assessments 7 (2014) 101–110. doi:https://doi.org/10.1016/j.seta.2014.04.002.

[7] S. P. Ayengo, H. Axelsen, D. Haberschusz, D. U. Sauer, A model for direct-coupled PV systems with batteries depending on solar radiation, temperature and number of serial connected PV cells, Solar Energy 183 (2019) 120–131. doi:https://doi.org/10.1016/j.solener.2019.03.010.

[8] G. F. Frate, P. P. Carro, L. Ferrari, U. Desideri, Techno-economic sizing of a battery energy storage coupled to a wind farm: an Italian case study, Energy Procedia 148 (2018) 447–454. doi:https://doi.org/10.1016/j.egypro.2018.08.119.

[9] L. Al-Ghussain, H. Ahmed, F. Haneef, Optimization of hybrid PV-wind system: Case study Al-Tafilah cement factory, Jordan, Sustainable Energy and Technologies Assessments 30 (2018) 24–36. doi:https://doi.org/10.1016/j.seta.2018.08.008.

[10] T. Ma, H. Yang, J. Peng, Technical feasibility study on a standalone hybrid solar-wind system with pumped hydro storage for a remote island in Hong Kong, Renewable Energy 69 (2014) 7–15. doi:https://doi.org/10.1016/j.renene.2014.03.028.

[11] T. Ma, M. S. Javed, Integrated sizing of hybrid PV-wind-battery system for remote island considering the saturation of each renewable energy resource, Energy Conversion and Management 182 (2019) 178–190. doi:https://doi.org/10.1016/j.enconman.2018.12.059.

[12] J. C. Alberizzi, M. Rossi, M. Renzi, A MILP algorithm for the optimal sizing of an off-grid hybrid renewable energy system in South Tyrol, Energy Reports 6 (2020) 21–26. doi:https://doi.org/10.1016/j.egyr.2019.08.012.

[13] D. B. Nelson, M. H. Nehrir, C. Wang, Unit sizing and cost analysis of standalone hybrid wind/PV/fuel cell power generation system, Renewable Energy 31 (2006) 1641–1656. doi:https://doi.org/10.1016/j.renene.2005.08.031.

[14] M. R. Elkadeem, S. Wang, S. W. Sharshir, E. G. Atia, Feasibility analysis and techno-economic design of grid-isolated hybrid renewable energy system for electrification of agriculture and irrigation area: A case study in Dongola, Sudan, Energy Conversion and Management 196 (2019) 1453–1478. doi:https://doi.org/10.1016/j.enconman.2019.06.085.

[15] W. Ma, X. Xue, G. Liu, R. Zhou, Techno-economic evaluation of a community-based hybrid renewable energy system considering site-specific nature, Energy Conversion and Management 171 (2018) 1737–1748. doi:https://doi.org/10.1016/j.enconman.2018.06.109.

[16] S. Singh, M. Singh, A. C. Kaushik, Feasibility study of an islanded microgrid in rural area consisting of PV, wind, biomass and battery energy storage system, Energy Conversion and Management 128 (2016) 178–190. doi:https://doi.org/10.1016/j.enconman.2016.09.046.

[17] M. Das, M. A. K. Singh, A. Biswas, Techno-economic optimization of an off-grid hybrid renewable energy system using metaheuristic optimization approaches – Case of a radio transmitter station in India, Energy Conversion and Management 185 (2019) 339–352. doi:https://doi.org/10.1016/j.enconman.2019.01.107.

[18] K. S. Krishna, K. S. Kumar, A review on hybrid renewable energy systems, Renewable and Sustainable Energy Reviews 52 (2015) 907–916. doi:https://doi.org/10.1016/j.rser.2015.07.187.

[19] J. Lian, Y. Zhang, C. Ma, Y. Yang, E. Chaima, A review on recent sizing methodologies of hybrid renewable energy systems, Energy Conversion and Management 199 (2019) 112027. doi:https://doi.org/10.1016/j.enconman.2019.112027.

[20] M. D. A. Al-falahi, S. D. G. Jayasinghe, H. Enshaei, A review on recent size optimization methodologies for standalone solar and wind hybrid renewable energy system, Energy Conversion and Management 143 (2017) 252–274. doi:https://doi.org/10.1016/j.enconman.2017.04.019.

[21] R. Ooka, S. Ikeda, A review on optimization techniques for active thermal energy storage control, Energy and Buildings 106 (2015) 225–233. doi:https://doi.org/10.1016/j.enbuild.2015.07.031.

[22] H. Morais, P. Kádár, P. Faria, Z. A. Vale, H. M. Khodr, Optimal scheduling of a renewable micro-grid in an isolated load area using mixed-integer linear programming, Renewable Energy 35 (2010) 151–156. doi:https://doi.org/10.1016/j.renene.2009.02.031.

[23] L. Ferrer-Martí, B. Domenech, A. García-Villoria, R. Pastor, A MILP model to design hybrid wind–photovoltaic isolated rural electrification projects in developing countries, European Journal of Operational Research 226 (2013) 293–300. doi:https://doi.org/10.1016/j.ejor.2012.11.018.

[24] A. Malheiro, P. M. Castro, R. M. Lima, A. Estanqueiro, Integrated sizing and scheduling of wind/pv/diesel/battery isolated systems, Renewable Energy 83 (2015) 646–657. doi:https://doi.org/10.1016/j.renene.2015.04.066.

[25] B. Zhao, X. Zhang, P. Li, K. Wang, M. Xue, C. Wang, Optimal sizing, operating strategy and operational experience of a stand-alone mi-

crogrid on Dongfushan island, Applied Energy 113 (2014) 1656–1666. doi:https://doi.org/10.1016/j.apenergy.2013.09.015.

[26] A. Stoppato, G. Cavazzini, G. Ardizzon, A. Rossetti, A PSO (particle swarm optimization)-based model for the optimal management of a small PV(Photovoltaic)-pump hydro energy storage in a rural dry area, Energy 76 (2014) 168–174. doi:https://doi.org/10.1016/j.energy.2014.06.004.

[27] G. Bekele, G. Tadesse, Feasibility study of small Hydro/PV/Wind hybrid system for off-grid rural electrification in Ethiopia, Applied Ene-Hybrid Optimization of Multiple Energy Resourcesrgy 97 (2012) 5–15. doi:https://doi.org/10.1016/j.apenergy.2011.11.059.

[28] H. Zahboune, S. Zouggar, G. Krajacic, P. S. Varbanov, M. Elhafyani, E. Ziani, Optimal hybrid renewable energy design in autonomous system using modified electric system cascade analysis and homer software, Energy Conversion and Management 126 (2016) 909–922. doi:https://doi.org/10.1016/j.enconman.2016.08.061.

[29] M. L. Kolhe, K. I. U. Ranaweera, A. S. Gunawardana, Techno-economic sizing of off-grid hybrid renewable energy system for rural electrification in Sri Lanka, Sustainable Energy Technologies and Assessments 11 (2015) 53–64. doi:https://doi.org/10.1016/j.seta.2015.03.008.

[30] M. Mehrpooya, M. Mohammadi, E. Ahmadi, Techno-economic-environmental study of hybrid power supply system: A case study in Iran, Sustainable Energy Technologies and Assessments 25 (2018) 1–10. doi:https://doi.org/10.1016/j.seta.2017.10.007.

[31] IHOGA, Simulation and optimization of stand-alone and grid-connected hybrid renewable systems, `https://ihoga.unizar.es/en/`, [Accessed: 2020-03-24].

[32] J. B. Fulzele, M. B. Daigavane, Design and Optimization of Hybrid PV-Wind Renewable Energy System, Materials Today Proceedings 5 (2018) 810–818. doi:https://doi.org/10.1016/j.matpr.2017.11.151.

[33] R. Dufo-López, J. L. Bernal-Augustín, J. M. Yusta-Loyo, J. A. Domínguez-Navarro, I. J. Ramírez-Rosado, J. Lujano, I. Aso, Multi-objective optimization minimizing cost and life cycle emissions of stand-alone pv–wind–diesel

systems with batteries storage, Applied Energy 88 (2011) 4033–4041. doi:https://doi.org/10.1016/j.apenergy.2011.04.019.

[34] MathWorks, Linear programming and mixed-integer linear programming, https://uk.mathworks.com/help/optim/index.html, [Accessed: 2020-04-20].

[35] F. Domínguez-Muñoz, J. M. Cejudo-López, A. Carrillo-Andrés, M. Gallardo-Salazar, Selection of typical demand days for CHP optimization, Energy and Buildings 111 (2011) 3036–3043. doi:https://doi.org/10.1016/j.enbuild.2011.07.024.

[36] A. Piacentino, C. Barbaro, A comprehensive tool for efficient design and operation of polygeneration-based energy grids serving a cluster of buildings. Part II: Analysis of the applicative potential, Applied Energy 111 (2013) 1222–1238. doi:https://doi.org/10.1016/j.apenergy.2012.11.079.

[37] A. Piacentino, C. Barbaro, F. cardona, R. Gallea, E. Cardona, A comprehensive tool for efficient design and operation of polygeneration-based energy grids serving a cluster of buildings. Part I: Description of the method, Applied Energy 111 (2013) 1204–1221. doi:https://doi.org/10.1016/j.apenergy.2012.11.078Get rights and content.

[38] PVGIS, Photovoltaic geographical information system, http://re.jrc.ec.europa.eu/pvgis.html, [Accessed: 2020-03-24].

[39] C. Brandoni, M. Renzi, Optimal sizing of hybrid solar micro-CHP systems for the household sector, Applied Thermal Engineering 75 (2015) 896–907. doi:https://doi.org/10.1016/j.applthermaleng.2014.10.023.

[40] Sharp, Sharp ND-R240A6 module, http://sharp-afg.com/?product=nd-r240a6, [Accessed: 2020-03-24].

[41] Homer-Energy, Wind resource variation with height, https://www.homerenergy.com/products/pro/docs/3.11/windresourcevariationwithheight.html, [Accessed: 2020-03-24].

[42] The Engineering ToolBox, Resources, tools and basic information for engineering and design of technical applications, https://www.

engineeringtoolbox.com/standard-atmosphere-d 604.html, [Accessed: 2020-03-24].

[43] C. Caligiuri, M. Renzi, M. Bietresato, M. Baratieri, Experimental investigation on the effects of bioethanol addition in diesel-biodiesel blends on emissions and performances of a micro-cogeneration system, Energy Conversion and Management 185 (2019) 55–65. doi:https://doi.org/10.1016/j.enconman.2019.01.097.

[44] A. Kaabeche, R. Ibtiouen, Techno-economic optimization of hybrid photovoltaic/wind/diesel/battery generation in a stand-alone power system, Solar Energy 103 (2014) 171–182. doi:https://doi.org/10.1016/j.solener.2014.02.017.

[45] IBM Knowledge Center, What is mixed integer-linear programming?, https://www.ibm.com/support/knowledgecenter/, [Accessed: 2020-03-24].

[46] Pembina Institute, The true cost of energy in remote communities, https://www.pembina.org/pub/diesel-true-cost, [Accessed: 2020-05-01].

[47] European Commission, Study on the implementation of article 7(3) of the "directive on the deployment of alternative fuels infrastructure" – fuel price comparison, https://ec.europa.eu/transport/sites/transport/files/2017-01-fuel-price-comparison.pdf, [Accessed: 2020-05-01].

[48] R. Lamedica, E. Santini, A. Ruvio, L. Palagi, I. Rossetta, A milp methodology to optimize sizing of PV - wind renewable energy systems, Energy 165 (2018) 385–398. doi:https://doi.org/10.1016/j.energy.2018.09.087.

[49] P. Hevia-koch, H. K. Jacobsen, Comparing offshore and onshore wind development considering acceptance costs, Energy Policy 125 (2019) 9–19. doi:https://doi.org/10.1016/j.enpol.2018.10.019.

[50] E. L. V. Eriksson, E. M. Gray, Optimization of renewable hybrid energy systems - A multi-objective approach, Renewable Energy 133 (2019) 971–999. doi:https://doi.org/10.1016/j.renene.2018.10.053.

[51] R. Dufo-López, J. L. Bernal-Agustín, Design and control strategies of PV-Diesel systems using genetic algorithms, Solar Energy 79 (2005) 33–46. doi:https://doi.org/10.1016/j.solener.2004.10.004.